

Influence of martensite/austenite interfaces on bainite formation in low-alloy steels below M_s

Ravi, Ashwath M.; Navarro-López, Alfonso; Sietsma, Jilt; Santofimia, Maria J.

DOI

[10.1016/j.actamat.2020.02.003](https://doi.org/10.1016/j.actamat.2020.02.003)

Publication date

2020

Document Version

Final published version

Published in

Acta Materialia

Citation (APA)

Ravi, A. M., Navarro-López, A., Sietsma, J., & Santofimia, M. J. (2020). Influence of martensite/austenite interfaces on bainite formation in low-alloy steels below M_s . *Acta Materialia*, 188, 394-405.
<https://doi.org/10.1016/j.actamat.2020.02.003>

Important note

To cite this publication, please use the final published version (if applicable).
Please check the document version above.

Copyright

Other than for strictly personal use, it is not permitted to download, forward or distribute the text or part of it, without the consent of the author(s) and/or copyright holder(s), unless the work is under an open content license such as Creative Commons.

Takedown policy

Please contact us and provide details if you believe this document breaches copyrights.
We will remove access to the work immediately and investigate your claim.



Full length article

Influence of martensite/austenite interfaces on bainite formation in low-alloy steels below M_s

Ashwath M. Ravi*, Alfonso Navarro-López, Jilt Sietsma, Maria J. Santofimia

Department of Materials Science and Engineering, Delft University of Technology, Mekelweg 2, CD Delft 2628, the Netherlands

ARTICLE INFO

Article History:

Received 12 September 2019

Revised 10 January 2020

Accepted 2 February 2020

Available online 6 February 2020

Keywords:

Bainite

Kinetics

Nucleation

Isothermal heat treatments

ABSTRACT

Bainite formation in steels typically starts at austenite grain boundaries and continues through nucleation of bainite at newly formed bainitic ferrite/austenite interfaces. Recent experimental evidence has pointed out that austenite to bainite transformation can also proceed in the presence of martensite. Studies suggest that the presence of athermal martensite formed prior to bainite formation can accelerate the kinetics of bainite formation with the martensite/austenite interfaces acting as potential nucleation sites. In this work, a kinetic model based on the displacive mechanism of bainite formation is adapted to isolate the impact of martensite/austenite interfaces on the overall rate of bainite formation when bainite formation occurs in the presence of previously formed martensite. This adapted kinetic model is validated using dilatometer studies published in the literature on a silicon-containing low-carbon steel in which bainite formation experiments are performed both below and above the M_s temperature. The results suggest that the formalism of the existing kinetic theory can describe the effects of martensite/austenite interfaces on the bainite formation.

© 2020 Acta Materialia Inc. Published by Elsevier Ltd. This is an open access article under the CC BY-NC-ND license. (<http://creativecommons.org/licenses/by-nc-nd/4.0/>)

1. Introduction

In the quest to meet the ever-growing demands of the industry, multiphase steel microstructures with their outstanding mechanical properties have been the subject of considerable attention in the recent years. One of the main constituents of such microstructures is bainite [1–4]. The formation of bainite in steels is one of the most intensely researched topics in the field of metallurgy [1,5–12]. Bainite microstructures typically consist of an assembly of bainitic ferrite laths which are separated by untransformed austenite, martensite or cementite [1,13–15]. The thickness of the bainitic laths depends on the bainite formation temperature [16]. Typically, as the transformation temperature decreases, the bainitic laths tend to become finer [14–16]. It is well established in the literature that grain refinement in metallic materials can lead to improved strength and toughness [17–19]. The mechanism of bainite formation naturally leads to highly fine grained structures, thereby making bainitic microstructures a popular choice for materials for structural applications [15,18].

The reduction of bainite formation temperature, however, leads to slower transformation kinetics [20,21]. Currently, researchers are investigating several strategies to accelerate the bainite formation

kinetics [20]. Studies show that one of the strategies to improve the rate of bainite formation is through the formation of a small fraction of martensite prior to bainite formation [22–24]. Several studies show that quenching of samples to a temperature below the M_s temperature to form a limited fraction of martensite, followed by isothermal holding above the M_s temperature leads to acceleration of bainite formation when compared to transformation without prior quenching below M_s [23,24]. However, the mechanism for acceleration of kinetics is disputed. Kawata et al. [24] suggest that the enhancement of bainite kinetics is due to the faster nucleation of bainitic subunits on martensite/austenite interfaces. Veters et al. [22] argue that the initial pre-quenching favours further bainite formation by altering the austenite matrix for easier austenite to bainite transformation. On the other hand, Sourmail et al. [25] point out that although the overall heat treatment time for austenite decomposition was reduced, they observed no detectable acceleration in bainite formation due to the presence of martensite during the isothermal holding itself.

Studies have also been carried out to understand the effect of prior martensite on microstructural processes during isothermal holding below M_s temperatures [26–28]. Literature evidence shows that bainite formation can not only occur during the isothermal holding below the M_s temperature [26,27,29], but the prior martensite formation can also have a strong accelerating effect on the bainite formation [26]. However, other studies seem to indicate that the isothermal transformation product obtained during isothermal holding below the M_s temperature may not be bainite [30,31].

* Corresponding author. Present address: TATA Steel Research Development & Technology, 1970 CA IJmuiden, the Netherlands.

E-mail addresses: ashwath.ravi@tatasteeleurope.com (A.M. Ravi),

A.NavarroLopez@tudelft.nl (A. Navarro-López), J.Sietsma@tudelft.nl (J. Sietsma),

M.J.SantofimiaNavarro@tudelft.nl (M.J. Santofimia).

It is evident from these studies that several aspects regarding the effect of prior martensite on the kinetics of bainite formation are still unresolved. In order to further clarify these unresolved issues, it is important to analyse the kinetics of bainite formation with and without prior martensite formation. As mentioned above, bainite formation in steels (without prior martensite formation) has been studied extensively and several researchers have proposed kinetic models to describe bainite formation kinetics [32–37]. The authors of the present work also recently proposed a kinetic model to understand the various factors which describe the kinetics of bainite formation by assuming that bainite grows via a displacive and diffusionless mechanism [38]. Published results show that kinetic models based on the displacive and diffusionless theory of bainite formation can accurately simulate the bainite formation kinetics in most cases [33,35–39].

In this study, the formalism of the kinetic model proposed in [38] by the authors of the present work is modified and adapted to analyse the experimental results obtained for the kinetics of bainite formation both with and without prior martensite formation. The kinetic model considers that the evolution of bainite fraction with time is controlled by the nucleation of bainitic ferrite at austenite grain boundaries and at bainite/austenite interfaces which form as bainite formation progresses. In principle, bainite nucleation would occur at austenite grain boundaries and bainite/austenite interfaces even in the presence of pre-existing martensite. Therefore, the trends obtained for the model parameters during the comparison of experimental results with the proposed kinetic model must be applicable (and extrapolatable) to the entire range of temperatures at which bainite formation can occur. With the help of the analysis of the model parameters over a range of transformation temperatures for bainite formation, this work explores the interplay between different factors which affect the bainite formation kinetics in conditions both in the presence of and the absence of martensite. Such an analysis sheds light on the role of prior martensite during bainite formation and its impact on bainite kinetics.

2. Theory and modified model

2.1. Background and model description

According to the kinetic model proposed in [38], the rate of the bainite formation, df/dt , at a given time, t , is proportional to the overall rate of bainite nucleation. Bainite nucleation is a thermally activated process [35] and depends on parameters such as the carbon concentration of the austenite matrix, X_γ , as a function of bainite fraction, f , and the bainite formation temperature, T [20,35,39,40]. The quantities X_γ and f are related to the bulk carbon concentration of the steel, \bar{X} . According to the model proposed in [38], the rate of bainite formation can be given by

$$\frac{df}{dt} = (1-f) \left(\frac{T_0 - T}{T_{0\bar{X}} - T} \right) \left[1 + \exp\left(\frac{\Delta Q^*}{kT}\right) f \right] \kappa \quad (1)$$

where κ is

$$\kappa = C(T_h - T) \exp\left(-\frac{Q_C^*}{kT}\right) \quad (2)$$

C depends on the composition of the steel and the prior austenite grain size. T_h is the critical temperature below which bainite nucleation can occur [41] while T_0 is the critical temperature below which bainite growth can occur according to the displacive theory of bainite formation [1,41]. $T_{0\bar{X}}$ is the T_0 temperature when the carbon concentration of austenite is equal to the bulk carbon content of the steel. The factor $T_h - T$ gives the undercooling which defines the driving force for bainite nucleation from austenite [41]. The factor $\left(\frac{T_0 - T}{T_{0\bar{X}} - T}\right)$ accounts for the thermodynamic condition required for the diffusionless growth of bainite [38].

The activation energy for bainite nucleation depends on the interface at which nucleation occurs [38]. In Eqs. (1) and (2), Q_C^* is the activation energy for bainite nucleation at austenite grain boundaries which can be related to the activation energy for autocatalytic nucleation (bainite nucleation at already formed bainite/austenite interfaces), Q_A^* , using ΔQ^* , by [38]

$$\Delta Q^* = Q_C^* - Q_A^* \quad (3)$$

The factor $(1-f)$ in Eq. (1) gives the residual austenite fraction in which bainite formation can take place. As bainite formation progresses, the residual austenite fraction decreases along with the available austenite grain boundary area for further bainite nucleation. Physically, the factor $(1-f)$ accounts for the decreasing austenite grain boundary area. The number density of autocatalytic nucleation sites depends, however, on the bainite/austenite interfaces. The density of bainite/austenite interfaces initially increases as the bainite fraction increases and then decreases as the austenite grain becomes increasingly consumed. As proposed in [38], the density of bainite/austenite interfaces can be accounted for by the factor $(1-f)f$.

It should be noted that the bainite formation in steels can be accompanied by carbon enrichment of surrounding austenite. This carbon enrichment of austenite affects the parameters such as T_0 , T_h and Q_C^* [38], gradually changing them during the bainite formation.

2.2. Physical parameters of the kinetic model

The kinetic model [38] uses the following physical parameters that can be determined by modeling the experimentally obtained kinetics.

2.2.1. Carbon content in bainite, X_b

In the kinetic model given in [38], the carbon concentration within the austenite matrix, X_γ , is calculated based on the overall carbon content, \bar{X} , the bainite fraction and the carbon content of the bainite, X_b . It must be noted that bainite can be classified as an aggregate of bainitic ferrite sub-units and carbides [13] depending on the chemical composition of the steel and bainite formation temperature. This implies that X_b accounts for the carbon in bainitic ferrite and in carbides including carbon trapping in defects. A simple mass balance shows that X_γ , as a function of X_b and f , can be given as [38]

$$X_\gamma = \frac{(\bar{X} - fX_b)}{(1-f)} \quad (4)$$

2.2.2. Initial activation energy for grain boundary nucleation, Q_{GX}^*

In order to accurately determine the activation energy for nucleation as a function of f , it is important to estimate the initial activation energy for austenite grain-boundary bainite nucleation, Q_{GX}^* (i.e., Q_C^* at $X_\gamma = \bar{X}$). Using the physical parameter Q_{GX}^* , the activation energy for bainite nucleation at austenite grain boundaries as a function of X_γ is given in [38] as

$$Q_C^* = Q_{GX}^* + K_\Gamma C_1 (X_\gamma - \bar{X}) \quad (5)$$

where $K_\Gamma C_1$ is the proportionality constant relating the activation energy for bainite nucleation to the carbon enrichment of austenite. $K_\Gamma C_1$ can be calculated according to the procedure described in [38]. It depends on the undercooling below the T_h temperature.

2.2.3. Difference in activation energy for grain-boundary and autocatalytic nucleation, ΔQ^*

Similar to Q_{GX}^* , it is necessary to determine the initial activation energy for autocatalytic nucleation, Q_{AX}^* (i.e., Q_A^* at $X_\gamma = \bar{X}$), to accurately model the bainite kinetics. Q_{AX}^* can be determined by using the parameter ΔQ_X^* which is the difference between the two activation energy values at the start of the transformation (ΔQ^* at $f = 0$ or

$X_\gamma = \bar{X}$). As noted before, the activation energy for bainite nucleation increases with increasing carbon enrichment of austenite (which increases with increasing bainite fraction if $X_b < \bar{X}$) [34,39]. However, due to the differences in the nature of the interfaces, carbon enrichment of the austenite during bainite formation will have different influences on the activation energies for grain-boundary and autocatalytic nucleation [42]. Furthermore, factors such as the instantaneous deformation state of the austenite in the vicinity of the bainite/austenite interfaces can be expected to affect the autocatalytic bainite nucleation as well [42]. Accounting for these factors, ΔQ^* can be given by

$$\Delta Q^* = \Delta Q_{\bar{X}}^* + \theta f \quad (6)$$

where the parameter θ quantifies the difference between the activation energy for autocatalytic bainite nucleation and grain-boundary nucleation as a function of bainite fraction [42].

2.3. Modifications to account for pre-existing martensite during bainite formation

One of the most important factors which influences the kinetics of bainite formation is the transformation temperature at which bainite forms. The effect of transformation temperature is well accounted for using the kinetic model proposed in the above sections [38]. However, during bainite formation after quenching the steel below the M_s temperature, the presence of pre-existing martensite also affects the rate of bainite formation. Studies suggest that during treatments where austenite is quenched to form a certain fraction of martensite prior to bainite formation, martensite/austenite interfaces can also act as nucleation sites for bainite formation [22,24,26]. Thus, the overall bainite formation rate at any given moment in the presence of pre-existing martensite can then be given as

$$\frac{df}{dt} = \left(\frac{df}{dt}\right)_M + \left(\frac{df}{dt}\right)_G + \left(\frac{df}{dt}\right)_A \quad (7)$$

where $(df/dt)_M$ gives the rate of bainite formation due to nucleation at martensite/austenite interfaces, $(df/dt)_G$ gives the rate of bainite formation due to nucleation at austenite grain boundaries and $(df/dt)_A$ gives the rate of autocatalytic bainite formation.

Typically, bainite formation begins at austenite grain boundaries and then continues autocatalytically at bainite/austenite interfaces. In the presence of pre-existing martensite, bainite can also nucleate at martensite/austenite interfaces following which bainite nucleation can proceed autocatalytically at newly formed bainite/austenite interfaces. This implies that the presence of martensite/austenite interfaces can be a source of additional autocatalytic nucleation sites and therefore can increase the rate of autocatalytic nucleation. Hence, Eq. (7) can be further expanded as,

$$\begin{aligned} \frac{df}{dt} &= \left(\frac{df}{dt}\right)_M + \left(\frac{df}{dt}\right)_G + \left(\frac{df}{dt}\right)_A \\ &= \left(\frac{df}{dt}\right)_M + \left(\frac{df}{dt}\right)_G + \left[\left(\frac{df}{dt}\right)_{AM} + \left(\frac{df}{dt}\right)_{AG}\right] \end{aligned} \quad (8)$$

where $(df/dt)_{AM}$ gives the rate of bainite formation due to nucleation at bainite/austenite interfaces which are formed due to bainite nucleation at martensite/austenite interfaces and $(df/dt)_{AG}$ gives the rate of bainite formation due to nucleation at bainite/austenite interfaces which are formed due to bainite nucleation at austenite grain boundaries. In the absence of martensite/austenite interfaces, $(df/dt)_{AM}$ would be 0 and autocatalytic nucleation would be determined by $(df/dt)_{AG}$ alone.

The rate of bainite formation is directly proportional to the density of potential nucleation sites which depends on the density of interfaces. As the bainite formation progresses, the nucleation sites are consumed at various interfaces. If the pre-existing martensite

has an accelerating effect on the kinetics of bainite formation as observed in the literature [22–24], it can be postulated that bainite nucleation will take place at the martensite/austenite interfaces when bainite formation occurs after quenching below the M_s temperature. Additionally, martensite/austenite interfaces would be consumed quicker than grain-boundary nucleation sites and autocatalytic nucleation sites under such circumstances. Once martensite/austenite interfaces are consumed due to bainite formation in its vicinity, $(df/dt)_M$ tends to zero and its influence on the overall bainite kinetics would diminish. Consequently, after a certain degree of bainite formation, the kinetics would be dominated by autocatalytic and grain-boundary bainite nucleation.

The kinetic model proposed in Section 2.1 is designed to capture the influence of autocatalytic bainite nucleation and grain-boundary bainite nucleation on the rate of bainite formation. Based on the above discussion, the proposed kinetic model can therefore be compared with experimentally determined bainite kinetics obtained from later stages of bainite formation (when $(df/dt)_M \approx 0$) where austenite to bainite transformation no longer occurs from martensite/austenite interfaces. The analysis will give the specific values for the physical parameters (discussed in Section 2.2) used by the kinetic model. With the help of the parameters obtained, the contributions of $(df/dt)_A$ and $(df/dt)_G$ on the overall rate of bainite formation over the entire isothermal holding time for bainite formation can be calculated. Using these calculations and the experimentally obtained bainite formation kinetics, the influence of martensite/austenite interfaces on the bainite formation $((df/dt)_M)$ can be subsequently isolated using Eqs. (7) and (8).

In order to determine the contributions of $(df/dt)_G$ and $(df/dt)_A$ when bainite formation occurs in the presence of martensite, the effect of pre-existing martensite fraction, f_M , on $(df/dt)_G$ and $(df/dt)_A$ should be incorporated into the model. It should be noted along with direct impact of f_M on the rate of bainite formation, as given by $(df/dt)_M$, f_M also influences the available austenite fraction in which bainite formation can occur. As mentioned previously, the density of grain-boundary and autocatalytic nucleation sites depends on the fraction of available austenite. Thus, it can be summarized that f_M has an effect on $(df/dt)_G$ and $(df/dt)_A$. The effect of f_M on the volume fraction of available austenite and on subsequent bainite autocatalytic nucleation or grain-boundary nucleation would be similar to the effect of the bainite fraction during typical bainite formation without any pre-existing martensite. Therefore, since f and f_M have a similar effect on the rate of bainite formation, the factor f in Eqs. (1), (4) and (6) can be replaced with $(f + f_M)$ in order to incorporate the effects of pre-existing martensite on the bainite kinetics. The presence of martensite would also affect the carbon enrichment of austenite since martensite can trap carbon either in form of carbides (tempered martensite) or as supersaturated martensitic ferrite (as shown in Section 4.4). As mentioned in Section 2.1, T_0 , T_h and Q_G^* are a function of carbon concentration of austenite, X_γ , which varies as bainite formation progresses. It should be noted that if the factor f is replaced with $(f + f_M)$ while calculating X_γ in Eq. (4), T_0 , T_h and Q_G^* values will vary accordingly.

3. Experiments

Dilatometer studies carried out in [26] were used to validate the modified model proposed in this work. A steel with nominal composition Fe-0.2C-3.52Mn-1.52Si-0.25Mo-0.04Al (in wt-%) (or, Fe-0.91C-3.49Mn-2.96Si-0.04Mo-0.08Al (in at-%)) was used in the study.

Dilatometer samples were first completely austenized at 900 °C for 4 min. The experimentally obtained M_s temperature of the steel is approximately 320 °C. The samples were then quenched to and isothermally held at temperatures ranging from 370 °C to 270 °C for 1 h. Finally, the samples were quenched to room temperature. It should be noted that during isothermal bainite treatments below the M_s

temperature, a certain fraction of athermal martensite will have already formed prior to the start of bainite formation. The detailed experimental procedure is given in [26].

Optical microscopy and scanning electron microscopy was carried out to understand the microstructural evolution within the samples as a result of the heat treatments [26]. Microstructural studies revealed the possibility of macrosegregation of Mn within the steel used in this study (shown in Section 4.1). Electron probe microanalysis (EPMA) experiments were carried out to investigate the macrosegregation of Mn and to understand the distribution of alloying elements within the steel.

4. Results and discussion

4.1. Experimental results

The experimentally determined evolution of bainite fraction under different isothermal conditions as a function of time is given in Fig. 1. The detailed procedure for the calculation of the reported volume fraction of bainite as well as martensite formed prior to bainite formation is described in [26]. The experimentally obtained bainite fraction at the end of the isothermal steps and the martensite fractions prior to bainite formation are given in Table 1 as well.

Fig. 1 (a) shows the evolution of bainite fraction as a function of time in the absence of previously formed martensite, while Fig. 1(b)

Table 1

Experimentally determined bainite fraction at the end of the isothermal treatment, f_{exp} and the martensite fraction formed during the initial quench from austenization temperature, f_M .

T [°C]	f_{exp}	f_M
370	0.62	0
340	0.74	0
330	0.83	0
320	0.84	0
310	0.82	0.04
300	0.71	0.16
270	0.12	0.77

shows the bainite formation kinetics in the presence of previously formed martensite. In Fig. 1(b), the value on the y-axis at the start of the treatment gives the fraction of martensite formed prior to the isothermal treatment. The x-axis gives the holding time at the isothermal step during which bainite formation occurs. The isothermal step is considered to start (time = 0 on the x-axis) at the moment the prior cooling step, from the austenization temperature, terminates. It should be noted that although the dilatometer is programmed to terminate the aforementioned cooling step at the intended isothermal bainite formation temperature, this is not exactly realized during the experiments. A small undercooling (2–5 °C) below the intended isothermal temperature is usually observed. However, the sample

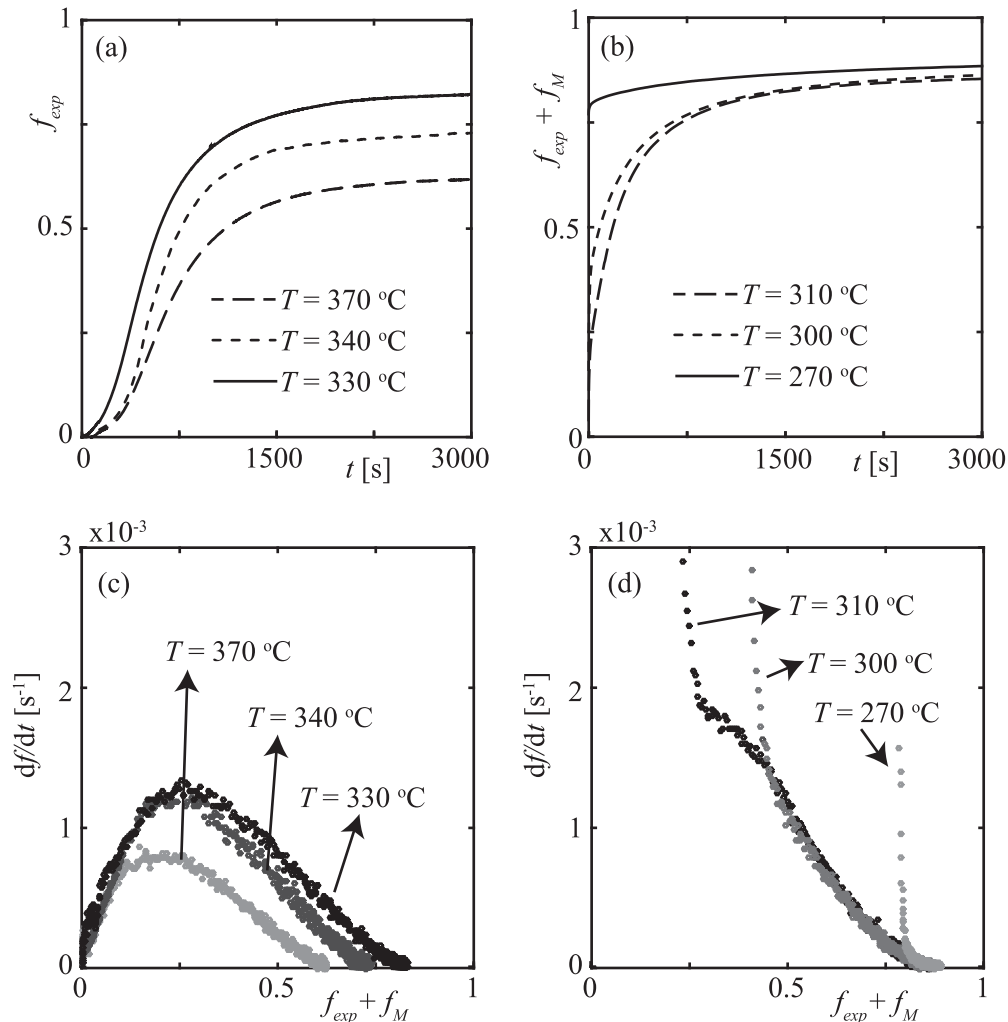


Fig. 1. Experimentally obtained bainite fraction, f_{exp} , as a function of time, t , (a) in the absence of any athermal martensite, i.e. below M_s conditions and (b) in the presence of pre-formed athermal martensite, i.e. above M_s conditions. Experimentally obtained rate of bainite formation as a function of bainite+martensite fraction, ($f_{exp} + f_M$) (c) in the absence of any athermal martensite and (d) in the presence of pre-formed athermal martensite. The martensite fraction is 0 when $T > 320$ °C.

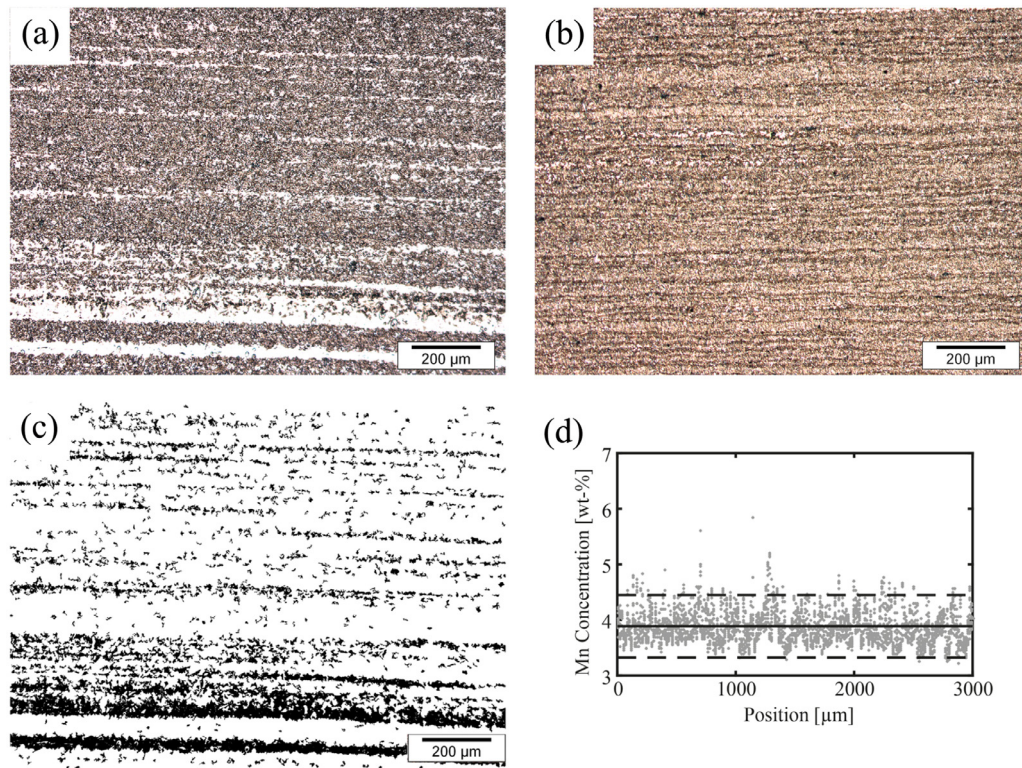


Fig. 2. (a) Microstructural evolution following bainite formation treatment at 370 °C. Banded microstructure can be seen with bainite (etched; dark) and austenite/martensite (unetched; white) regions (b) Microstructural evolution following bainite formation treatment at 310 °C. The severity of banding is reduced (fully etched; dark). (c) Areas (in black) indicating austenite resistant to bainite formation at 370 °C. This fraction of austenite is stabilized due to high Mn content in these regions. These black regions correspond to the white etched regions in (a). (d) EPMA results showing Mn distribution over a length of 3 mm within the steel used in the study

temperature quickly stabilizes to the intended temperature (± 0.1 °C) within a couple of seconds.

Based on Fig. 1(a) and Fig. 1(b), the rate of bainite formation as a function of bainite evolution in the absence and in the presence of previously formed martensite is calculated (Fig. 1(c) and Fig. 1(d)). It should be stated that since Fig. 1(c) and Fig. 1(d) are plotted as a function of combined bainite and martensite fractions, the curves for the rate of bainite formation are shifted depending on the fraction of previously formed martensite (Table 1). The rate of bainite formation due to grain-boundary and autocatalytic nucleation is influenced by both bainite and martensite fraction when bainite forms in the presence of previously formed martensite as explained in Section 2.3. During bainite formation in the absence of martensite, it can be seen from Fig. 1(c) that the rate of bainite formation initially increases until a certain fraction of bainite is reached and then decreases as further bainite is formed. Furthermore in Fig. 1(d), it can be clearly seen that the presence of martensite fraction prior to bainite formation influences the rate of the bainite formation. During bainite formation in the presence of martensite, the rate of bainite formation is relatively high in the early stages of bainite formation. The rate of bainite formation rapidly decreases after certain fraction of bainite is formed and then follows a trend similar to the one observed when bainite forms without martensite. Comparing Fig. 1(c) and 1(d), it can be observed that the rate of bainite formation in the presence of martensite is typically higher almost throughout the bainite formation process. This can be seen especially in the case of bainite formation at 310 °C and 300 °C. Based on Fig. 1(d), a qualitative description for bainite formation process in the presence of previously formed martensite can be envisaged. When bainite forms in the presence of martensite, bainitic ferrite initially forms quickly, presumably at martensite/austenite interfaces, resulting in the fast initial bainite kinetics. Once these interfaces are consumed, the bainite formation proceeds at a speed controlled by grain-boundary bainite nucleation

and autocatalytic bainite nucleation which peaks again until a certain bainite fraction is reached and then the bainite formation slows down. This is similar to the trend seen when bainite forms in the absence of martensite where bainite forms only via grain-boundary nucleation and autocatalytic nucleation. This results in a peak (at $f_{exp} \approx 0.2-0.3$) (Fig. 1(c) in all cases and in Fig. 1(d) at 310 °C where $f_M = 0.04$). In case of bainite formation at 300 °C and 270 °C, the rate of bainite formation only slows down after initial fast kinetics due to the presence of martensite/austenite interfaces since the combined bainite-martensite fraction is too high ($f_{exp} + f_M > 0.2$). These results are in line with the assumptions proposed in Section 2.3 suggesting that $(df/dt)_M$ tends to zero after a certain fraction of bainite is formed. Furthermore, the higher overall rate of bainite formation in the presence of previously formed martensite even after $(df/dt)_M$ tends to zero can be attributed to the increase in density of nucleation sites. The presence of martensite/austenite interfaces leads to an increase in the rate of autocatalytic nucleation as discussed earlier (Eq. (8)). A further understanding of this trend is discussed in Section 4.2.

The results of the optical microscopy studies carried out on the samples obtained after various heat treatments is given in Fig. 2. These results show a certain degree of inhomogeneity in the microstructural evolution depending on the transformation temperature at which bainite formation occurs. At relatively high bainite formation temperatures (above 340 °C), a banded microstructure can be observed (Fig. 2(a)) where certain bands clearly show bainite while some bands appear to remain untransformed during the bainite formation stage and show only martensite/retained austenite microstructure. It must be noted that 2% Nital etchant was used to reveal the microstructures. Nital etches the bainitic regions while martensite and retained austenite regions remain unetched [43]. The banded microstructure is a result of inhomogeneous distribution of Mn within the steel as shown by EPMA results in Fig. 2(d), which is due to macrosegregation of Mn introduced during the casting and rolling

Table 2
Adjusted fraction of bainite considering inhomogeneous Mn distribution.

T [°C]	f_{exp}	f_{yu}	f_{ad}
370	0.62	0.18	0.75
340	0.74	0.08	0.80
330	0.83	0.01	0.84
320	0.84	0.01	0.85
310	0.82	0	0.82
300	0.71	0	0.71
270	0.12	0	0.12

of the as-received steel. Thermodynamic calculations indicate that the driving force for both bainite nucleation and bainite growth decreases as the Mn content increases. Furthermore, comparing Fig. 2(a) and Fig. 2(b), it can be seen that the severity of the banded microstructure, or in other words the resistance to bainite formation, decreases as the bainite formation temperature (T) decreases. Such a trend can be attributed to increasing undercooling (or increasing driving force, see Section 2.1) for both bainite growth and bainite nucleation for a given Mn distribution in the steel.

It is evident from the above discussion that Mn segregation results in certain fraction of stable austenite which resists bainite formation throughout the isothermal holding step, especially at higher bainite formation temperatures (as evidenced in Fig. 2(a)). Furthermore, this stable austenite fraction decreases with decreasing bainite formation temperature since the undercooling increases. This implies that the experimentally obtained bainite fraction is underestimated since bainite formation only proceeds within a limited austenite matrix and the degree of this underestimation varies with bainite formation temperature. Thus, in order to compare bainite kinetics obtained at various temperatures, the total volume fraction of bainite formed at a given transformation temperature is to be adjusted by considering only the fraction of austenite where bainite formation occurs. Physically, this adjusted fraction of bainite formed, f_{ad} , signifies the fraction of bainite that would have formed if bainite formation was not restricted by inhomogeneities in Mn distribution and it can be given by

$$f_{ad} = \frac{f_{exp}}{1 - f_{yu}} \quad (9)$$

where f_{exp} is the experimentally determined bainite fraction and f_{yu} is the Mn-rich austenite fraction which remains untransformed throughout the isothermal holding step. f_{yu} was determined by image analysis of micrographs obtained. Using the banded structure seen in optical micrographs (Fig. 2(a)), untransformed austenite bands during the isothermal bainite formation treatment can be isolated (black regions in Fig. 2(c)). It should be noted that the untransformed austenite from the bainite formation stage partially transforms into martensite during final cooling, leading to a retained austenite/untreated martensite microstructure (which can be identified in the optical micrographs). The volume fraction of these untransformed austenite bands during bainite formation, f_{yu} , is assumed to be equal to the area fraction of the black regions in Fig. 2(c). The experimentally determined volume fraction of bainite and the volume fraction of bainite after adjusting for Mn distribution (Eq. (9)) are tabulated in Table 2.

4.2. Comparison of experimental data with calculated kinetics

With the help of the modified kinetic model proposed in this work, the experimentally obtained bainite kinetics is compared with the modelled bainite kinetics (Figs. 3 and 4). The values for the various constants used for the model are given in Table 3. They were obtained using Thermo-Calc as well as different empirical equations [39,44], as mentioned in [38]. The final bainite fraction given in

Figs. 3 and 4 is based on the adjusted bainite fraction, f_{ad} , as tabulated in Table 2.

Fig. 3 shows the comparison between experimentally obtained and model derived bainite kinetics when the bainite formation temperature is above the M_s temperature (i.e., in the absence of martensite). It can be seen that the calculated and experimentally obtained kinetics agree well. It should be noted that the experimental kinetics was obtained using dilatometer experiments and over 7000 data points were recorded during the isothermal step where bainite formation occurs. Since the purpose of Fig. 3 and Fig. 4 is to highlight the good correlation between the model and the experimental data, only a few, but a representative set, of the experimentally obtained data points is shown.

The modified kinetic model is derived based on the nucleation kinetics of bainite at austenite grain-boundaries and bainite/austenite interfaces only. However, in the presence of martensite, bainite formation can occur at martensite/austenite interfaces as well which is not accounted for by the model. But, considering the results discussed in Section 4.1 and seen in Fig. 1(d), only the kinetic data pertaining to the initial stages which shows high rate of bainite formation is attributed to the bainite formation due nucleation at martensite/austenite interfaces. The rest of the kinetic data is controlled by bainite formation due to grain-boundary and autocatalytic nucleation and thus, this partial experimental data set (Fig. 4) is used to compare the experimentally obtained kinetics with the model when bainite is formed in the presence of martensite. It can be seen that the kinetic model fits well when compared with the experimentally obtained data once the martensite/austenite interfaces are consumed during bainite formation. In Fig. 4(b), Fig. 4(c) and Fig. 4(d), the dots give the experimentally obtained rate of bainite formation as a function of combined bainite-martensite fraction. The solid line gives the calculated rate of bainite formation according to the model when it is fitted to the partial experimental data set. The dashed lines in Fig. 4(b), Fig. 4(c) and Fig. 4(d) show the rate of bainite formation extrapolated over the entire time-scale of the bainite formation treatment based on the model parameters obtained using the partial fitting. Physically, this extrapolation gives the rate of bainite formation if it was only determined by autocatalytic nucleation and grain-boundary nucleation.

Based on results obtained in Figs. 3 and 4, a few important conclusions can be derived. Firstly, the existing kinetic theory based on the displacive mechanism of bainite formation [33–35,37,38] and the formalism of kinetic model proposed in [38] can be used to accurately describe the bainite formation kinetics in the presence of pre-existing martensite once a certain fraction of bainite is formed. Similar analysis has been proposed recently by Samanta et al. [28]. Secondly, any effect of pre-existing martensite on the kinetics of bainite formation fades once the bainite formation progresses.

Both the complete fitting (for data obtained above M_s temperature) and the partial fitting (for data obtained below M_s temperature) of the experimentally determined data with the kinetic model yields corresponding model parameters. Fig. 5(a) shows the Q_{GX}^* parameter as a function of undercooling ($T_h - T$). It can be seen that Q_{GX}^* decreases linearly with increasing undercooling. A linear trend compares well with similar results reported in the literature [1,37]. The authors in their previous work also found similar results [38]. It must be also noted in Fig. 5(a) that the linear trend obtained for the variation in Q_{GX}^* as a function of undercooling can be extrapolated to the entire temperature range where austenite to bainite formation is possible, regardless of the presence of pre-existing martensite. The linear trend (dashed line in Fig. 5(a)) is based only on Q_{GX}^* values obtained when bainite forms in the absence of martensite and the Q_{GX}^* values obtained when bainite forms in the presence of martensite falls along this linear trend.

Fig. 5(b) shows the variation in Q_{AX}^* as a function of undercooling ($T_h - T$). Similar to Fig. 5(a), Q_{AX}^* decreases linearly with increasing

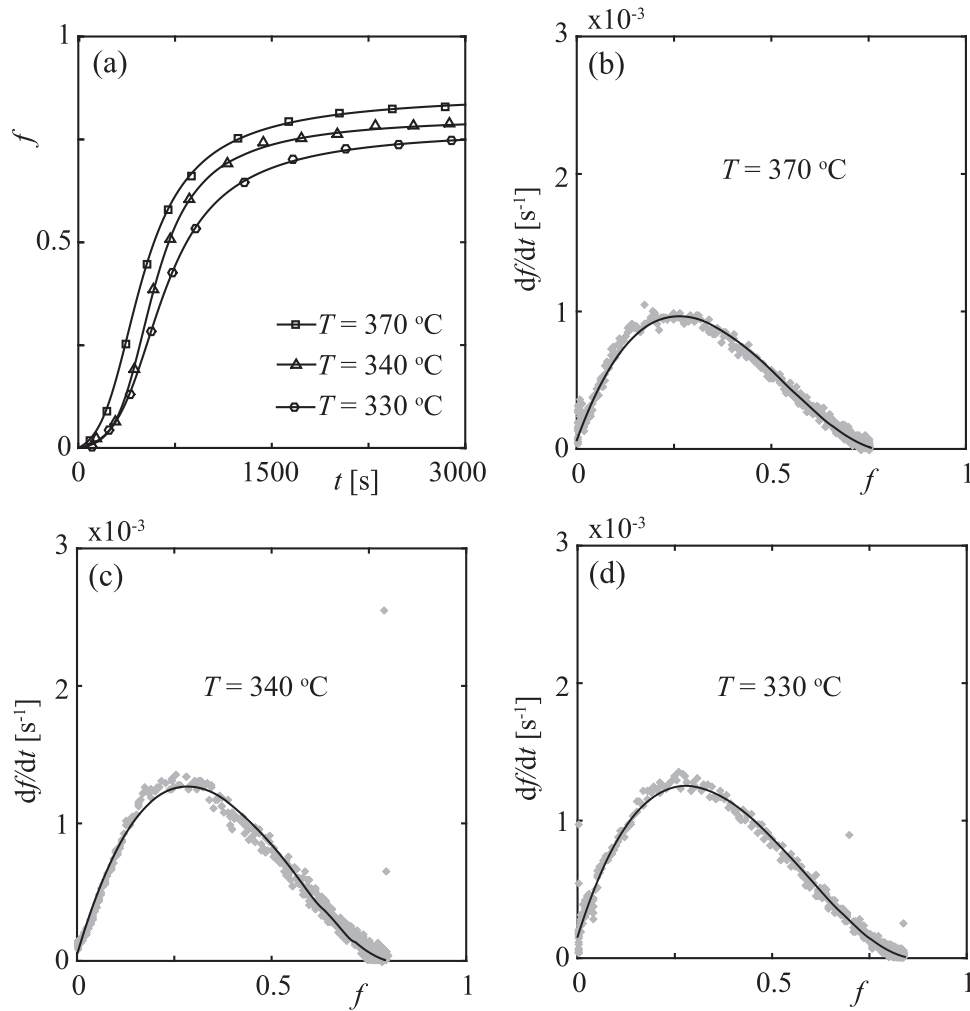


Fig. 3. Comparison of bainite kinetics. f_{ad} (markers) and model derived (lines) bainite fraction as a function of time, t , in the absence of any athermal martensite is given in (a). Experimentally determined (grey dots) and model derived (black solid lines) rate of bainite formation in the absence of any athermal martensite at various isothermal conditions is given in (b), (c) and (d).

undercooling when bainite formation occurs in the absence of martensite. However, unlike Fig. 5(a), the linear trend cannot be extrapolated to transformation temperatures where bainite formation occurs in the presence of martensite. As seen in Fig. 5(b), the calculated Q_{AX}^* values based on the obtained kinetic data is slightly below the predicted trend.

As mentioned earlier, in Section 4.1, the presence of previously formed martensite leads to an increased rate of autocatalytic nucleation. On the other hand, bainite nucleation at martensite/austenite interfaces would not have any effect on bainite nucleation at austenite grain boundaries. These can be considered as two separate events which will proceed based on local conditions at the respective interfaces. These observations are corroborated by results seen in Fig. 5. The variation in Q_{GX}^* as a function of undercooling (Fig. 5(a)) shows that the activation energy for grain-boundary nucleation does not depend on the presence of previously existing martensite and only depends on transformation temperature. This also serves as a validation for the values of fitting parameters obtained based on the partial fitting of experimental data with the proposed kinetic model. Fig. 5 (b) shows that autocatalytic nucleation is however influenced by the presence of previously existing martensite. It should be noted that the kinetic model proposed in Section 2 is used to calculate the Q_{GX}^* and Q_{AX}^* given in Fig. 5. As described previously, the model does not incorporate the influence of previously formed martensite and consequently does not account for increase in autocatalytic nucleation sites due to presence of martensite/austenite interfaces. Thus, when

compared with the experimental results, the model estimates a lower Q_{AX}^* when bainite forms below M_s to compensate for the underestimated autocatalytic nucleation sites and elucidate the increased rate of autocatalytic nucleation.

4.3. Impact of pre-existing martensite on bainite kinetics

Based on the results obtained in Sections 4.1 and 4.2, it is clear that the presence of martensite prior to bainite formation accelerates its kinetics. This acceleration is due to bainite nucleation at martensite/austenite interfaces as well as autocatalytic nucleation of bainite on bainite/austenite interfaces created during bainite formation at martensite/austenite interfaces (Eq. (8)).

Using Eq. (7), the rate of bainite formation due to bainite nucleation at martensite/austenite interfaces can be derived by estimating the difference between the experimentally obtained rate of bainite formation and the sum of $(df/dt)_G$ and $(df/dt)_A$. This difference is plotted (dots) as a function of bainite evolution in Fig. 6 with the help of calculations reported in Fig. 4(b–d). It should be noted that Fig. 4 (b–d) gives the experimentally obtained overall rate of bainite formation as well as the model estimated sum of $(df/dt)_G$ and $(df/dt)_A$. As already noted, the rate of bainite formation typically depends on two factors - activation energy for bainite nucleation and number density of nucleation sites. Published results on the crystallography of bainite and martensite suggest that both the bainite/austenite interfaces and the martensite/austenite interfaces are typically coherent or

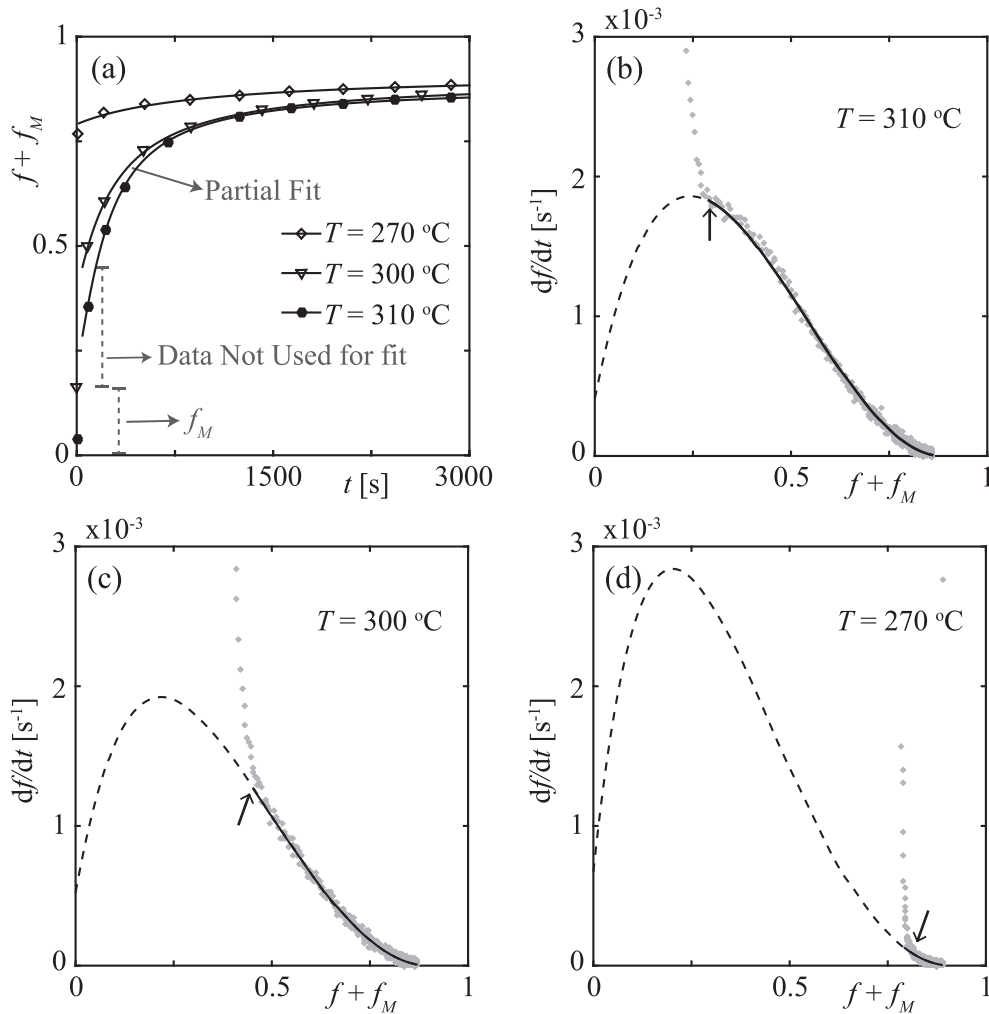


Fig. 4. Comparison of bainite kinetics. f_{ad} (markers) and model derived (lines) bainite fraction as a function of time, t , in the presence of previously formed athermal martensite is given in (a). Experimentally determined (grey dots) and model derived (solid black lines) rate of bainite formation in the presence of previously formed athermal martensite at various isothermal conditions is given in (b), (c) and (d). A partial fit is used to compare the model with experimental data. In (a), the solid line (model based results) do not cover all markers (experimental data) showing the length of the partial fit. This is highlighted with text as well for $T = 300$ °C case. Similar partial fit is used in all cases. In (b), (c) and (d), the solid black line shows the model calculated rate of bainite formation. Based on this fit, the rate of bainite formation is extrapolated (dashed black lines) to the entire data range to calculate the influence of autocatalytic and grain-boundary nucleation alone. The arrows in (b), (c) and (d) indicate the end of extrapolation and start of partial fit.

semi-coherent interfaces and show a defined orientation relationship (near Kurdjumov–Sachs or near Nishiyama–Wasserman relationship) [45,46]. Furthermore, at temperatures where bainite formation or martensite formation occurs, partitioning of substitutional solute atoms does not occur [47,48]. Based on the above mentioned similarities between bainite/austenite interfaces and martensite/austenite interfaces, it can be postulated that the activation energy for bainite nucleation at both these interfaces is similar. However, the number density of nucleation sites at bainite/austenite interfaces depends on the bainite fraction whereas the number density of nucleation sites at martensite/austenite interfaces depends on the previously formed

martensite fraction. With the help of the above discussion and using Fig. 6, the rate of bainite formation at martensite/austenite interfaces can be best fit using an exponential function as

$$\left(\frac{df}{dt}\right)_M = \frac{(df/dt)_A}{(1-f)f} (\beta_1 \exp(-\beta_2 f)) \quad (10)$$

where β_1 and β_2 are constants. It should be noted that the rate of bainite formation at martensite/austenite interfaces is given in terms of the rate of bainite formation due to autocatalytic nucleation. The factor $(1-f)f$ accounts for the number density of autocatalytic nucleation sites and the factor $\{(df/dt)_A/(1-f)f\}$ gives the rate of bainite formation due to autocatalytic nucleation per unit density of bainite/austenite interfaces. The factor $(\beta_1 \exp(-\beta_2 f))$ accounts for the density of nucleation sites at martensite/austenite interfaces. This factor is an exponential decay type expression. It is evident that as bainite nucleation continues at martensite/austenite interfaces, the density of nucleation sites at these interfaces decreases. Furthermore, along with bainite formation during the isothermal holding, tempering of martensite formed in the previous cooling step takes place. Thus, as time progresses (or equivalently, as bainite formation progresses), austenitic regions in the vicinity of martensite/austenite interfaces become carbon enriched and these interfaces become less favourable for bainite nucleation. It can thus

Table 3

Values for the constants used in relating experimental observation with the bainite formation model.

Parameter	Value	Reference
$T_{h\bar{x}}$	821 K	Thermo-Calc
C_1	2271 K/at.fr.	Thermo-Calc
$T_{0\bar{x}}$	818 K	Thermo-Calc
C_2	7165 K/at.fr.	Thermo-Calc
K_{Γ}	130 J/mol K	[39]
m	0.018 /K	[44]

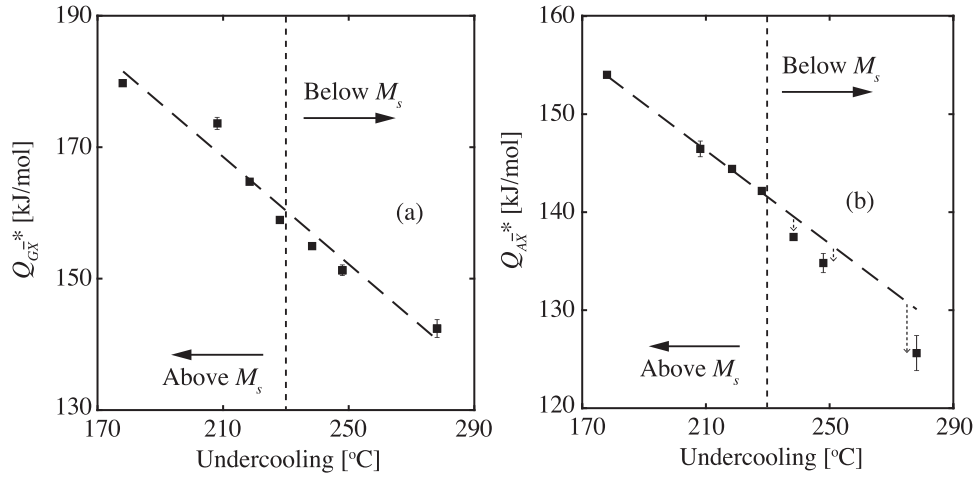


Fig. 5. Variation of (a) Q_{GX}^* and (b) Q_{AX}^* as a function of undercooling ($T_h - T$). Square data points give the respective activation energy values derived from the model fitting parameters. The dashed line represents the linear fit considering only the activation energy values obtained when bainite formation occurs in the absence of martensite. The error bar gives the 95% confidence interval. In case the error bar is not visible, the margin of error is less than 1 kJ/mol.

be postulated that both progress of bainite formation and martensite tempering lead to an exponential decay in the density of nucleation sites at martensite/austenite interfaces.

$(df/dt)_A$ can be calculated using the model given in Section 2 and the model parameters obtained in Section 4.2. Using Eq. (10) and Fig. 6, β_1 and β_2 are calculated for different bainite formation treatments carried out in the presence of previously formed martensite (Table 4). It can be noted that β_1 increases with increasing martensite fraction (decreasing bainite formation temperature). On the other hand, β_2 initially increases with increasing prior martensite fraction (decreasing bainite formation temperature) and then decreases when the martensite fraction is considerable (in this case $\approx 77\%$). These values indicate that the accelerating effect of martensite/austenite interfaces is considerable at the start of the bainite formation process and depends on the fraction of martensite present. This accelerating effect decreases exponentially as bainite formation continues. The exponential decay may be related to the availability of martensite/austenite interfaces whose density also initially increases with increasing martensite fraction and later decreases as a result of increasing austenite decomposition. Additionally, a higher initial martensite fraction implies that the subsequent carbon enrichment of austenite would be higher as well due to carbon partitioning from martensite to austenite during the isothermal step. This will increase the activation energy of bainite nucleation at martensite/austenite interfaces resulting in slower kinetics. This implies that the impact of previously formed martensite on bainite kinetics depends on the fraction of martensite present

which influences the density of nucleation sites where bainite can occur and the carbon concentration of the austenite. These factors determine the acceleration of bainite formation.

Based on Eq. (8), the total impact of pre-existing martensite on bainite kinetics can be quantified as the sum of $(df/dt)_M$ and $(df/dt)_{AM}$. Alternatively, the difference between the overall experimentally obtained rate of bainite formation and the sum of $(df/dt)_G$ and $(df/dt)_{AG}$ would give the impact of pre-existing martensite on bainite kinetics. The kinetic model described in Section 2 can be used to estimate the sum of the $(df/dt)_G$ and $(df/dt)_{AG}$ terms.

Fig. 5 gives the variation of Q_{GX}^* and Q_{AX}^* . It is evident that Q_{GX}^* determines $(df/dt)_G$ and Q_{AX}^* determines $(df/dt)_A$ [38,42]. Since $(df/dt)_{AM}$ is 0 when bainite formation is carried out in the absence of martensite/austenite interfaces, Q_{AX}^* determines $(df/dt)_{AG}$ under such conditions. Fig. 5(b) shows that Q_{AX}^* decreases linearly above M_s . Based on the above discussion, it can be postulated that if this linear trend based on above- M_s (in the absence of martensite) data points can be extrapolated, Q_{AX}^* predicted by this extrapolation can be used to determine $(df/dt)_{AG}$ at a given temperature below M_s (in the presence of martensite). This predicted Q_{AX}^* as well as the obtained Q_{GX}^* (Fig. 5(b)) is used to recalculate the bainite kinetics using the model given in Section 2. Physically, the results give the sum of $(df/dt)_{AG}$ and $(df/dt)_G$ terms which is the rate of bainite formation assuming that there is no influence of martensite formation at all. Fig. 7 gives a comparison between the predicted rate of bainite formation without any influence of pre-existing martensite and experimentally obtained kinetics when bainite forms below M_s temperatures.

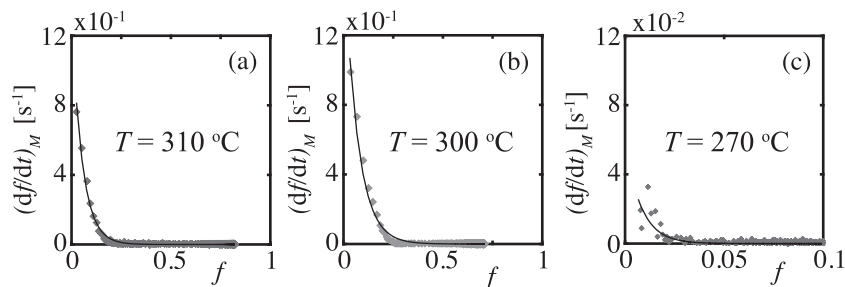


Fig. 6. Impact of previously formed martensite on subsequent rate of bainite formation which is calculated as the difference between the experimentally determined rate of bainite formation and the sum of $(df/dt)_G$ and $(df/dt)_{AG}$ when bainite forms at (a) $T = 310$ °C, (b) $T = 300$ °C and (c) $T = 270$ °C. The dots give the calculated difference and the solid line represents an exponential fit of the calculated difference.

Table 4
 β_1 and β_2 values obtained as a function of bainite formation temperature.

T [°C]	f_M	β_1	β_2
310	0.04	9	17
300	0.16	15	11
270	0.77	101	290

4.4. Physical parameter X_b

Table 5 shows X_b as a function of bainite formation temperature. It can be seen in Table 5 that X_b is higher at lower bainite formation temperatures. Microstructural observations detailed in [26] show that when bainite formation occurs above 340 °C in the steel studied in this work, cementite precipitation is completely suppressed. However, as bainite formation temperature decreases, the possibility of lower-bainite formation increases. Furthermore, as the bainite formation temperature drops below the M_s temperature, austenite also decomposes into martensite prior to bainite formation. The X_b values shown in Table 5 are in line with these results. If cementite formation is completely suppressed, the amount of carbon trapped within bainite would be relatively low and more carbon would be available for carbon enrichment of surrounding austenite. Therefore, the X_b value would be relatively low as well. As the probability of lower-bainite

Table 5
 X_b values obtained as a function of bainite formation temperature, T ($\bar{X} = 0.91$ at%). The calculated standard error of the X_b values is less than 0.03 at%.

T [°C]	X_b [at%]
370	0.164
340	0.187
330	0.405
320	0.466
310	0.433
300	0.489
270	0.520

formation increases and/or as more martensite formation occurs, the amount of carbon available for carbon enrichment of the austenite will be lower since more carbon would become trapped within the bainitic or martensitic regions. This would result in a higher X_b value.

5. Conclusions

The studies carried out in this work show that the existing kinetic theory for displacive bainite formation can be used to describe grain-boundary and autocatalytic bainite formation both in the presence of and absence of martensite. Using the existing kinetic theory for

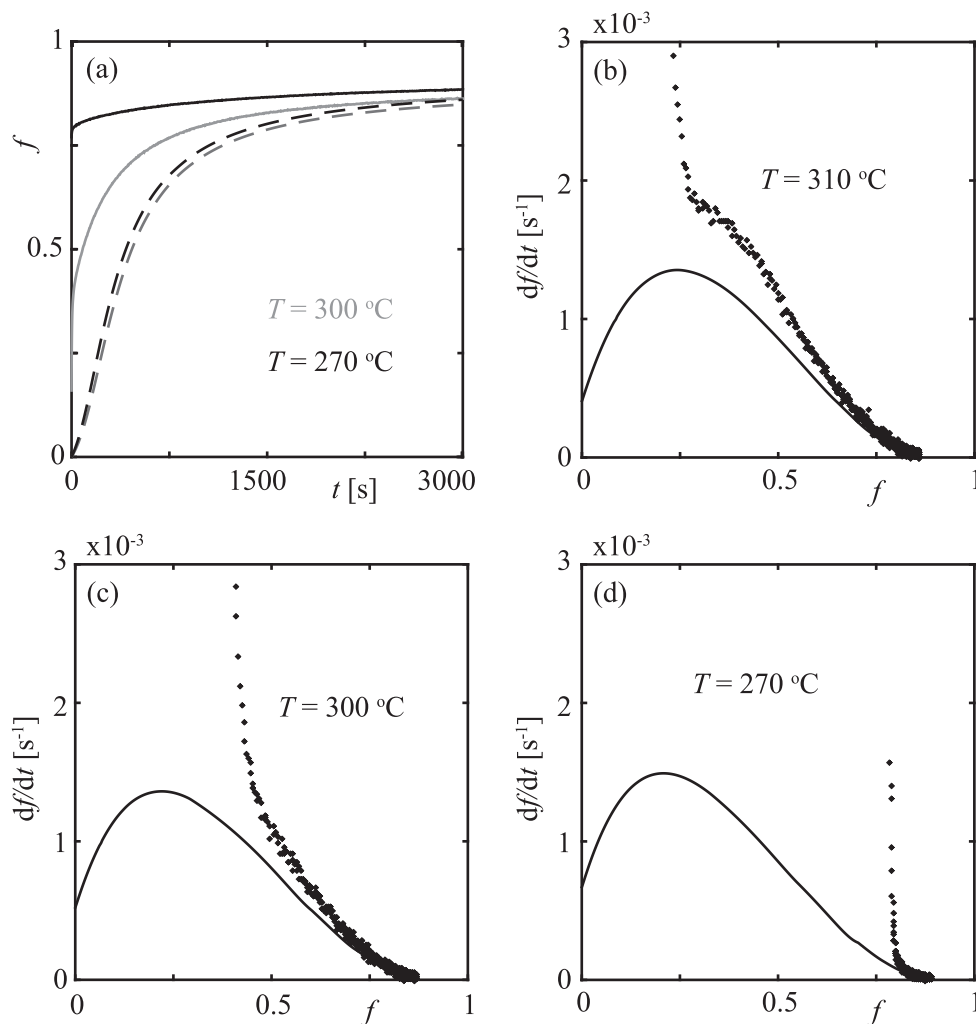


Fig. 7. Experimentally determined (solid line) bainite evolution in the presence of previously formed athermal martensite and model predicted (dashed line) bainite evolution excluding the influence of previously formed martensite on bainite kinetics is given in (a). In (a), grey lines indicate the case when $T = 300$ °C while black line represent the case when $T = 270$ °C. Experimentally determined (dots) rate of bainite formation in the presence of martensite and calculated (lines) rate of bainite formation excluding the influence of previously formed martensite at various isothermal conditions is given in (b), (c) and (d).

bainite formation, the role of martensite/austenite interfaces on the overall rate of bainite formation is isolated and quantified in detail. An equation to describe the rate of bainite nucleation at martensite/austenite interfaces has been proposed in this work.

The results indicate that bainite formation in the presence of previously formed martensite begins at both austenite grain boundaries as well as martensite/austenite interfaces. The rate of bainite formation at martensite/austenite interfaces does not affect bainite formation at austenite grain boundaries. However, bainite formation at martensite/austenite interfaces leads to the creation of bainite/austenite interfaces which can facilitate autocatalytic nucleation. The role of the martensite/austenite interfaces on the rate of bainite nucleation is closely dependent on the fraction of the pre-existing martensite. The fraction of pre-existing martensite can affect both the number density of nucleation sites and carbon enrichment of austenite. As the pre-existing martensite fraction increases, the rate at which bainite formation starts, increases. However, the overall rate of bainite formation decreases quickly as the available martensite/austenite interfaces are consumed and carbon enrichment of austenite increases due to carbon partitioning from martensite to austenite.

Declaration of Competing Interests

The authors declare that they have no known competing financial interests or personal relationships that could have appeared to influence the work reported in this paper.

Acknowledgements

The research leading to these results has received funding from the European Research Council under the European Union's Seventh Framework Programme (FP/2007-2013) / ERC Grant Agreement n. [306292].

References

- [1] H.K.D.H. Bhadeshia, *Bainite in Steels: Transformations, Microstructure and Properties*, *Matsci Series*, IOM Communications, 2001.
- [2] F.G. Caballero, H.K.D.H. Bhadeshia, Very strong bainite, *Current Opin. Solid State Mater. Sci.* 8 (3–4) (2004) 251–257, doi: [10.1016/j.cossms.2004.09.005](https://doi.org/10.1016/j.cossms.2004.09.005).
- [3] H.K.D.H. Bhadeshia, Nanostructured bainite, *Proceedings of the R. Soc. Lond. A Math. Phys. Eng. Sci.* 466 (2113) (2009) 3–18, doi: [10.1098/rspa.2009.0407](https://doi.org/10.1098/rspa.2009.0407).
- [4] B.C. de Cooman, Structure-properties relationship in TRIP steels containing carbide-free bainite, *Current Opin. Solid State Mater. Sci.* 8 (3–4) (2004) 285–303, doi: [10.1016/j.cossms.2004.10.002](https://doi.org/10.1016/j.cossms.2004.10.002).
- [5] H.K.D.H. Bhadeshia, D.V. Edmonds, The mechanism of bainite formation in steels, *Acta Metallurgica* 28 (9) (1980) 1265–1273, doi: [10.1016/0001-6160\(80\)90082-6](https://doi.org/10.1016/0001-6160(80)90082-6).
- [6] W.T. Reynolds Jr., H.I. Aaronson, G. Spanos, A summary of the present diffusionist views on bainite, *Mater. Trans. JIM* 32 (8) (1991) 737–746, doi: [10.2320/matertrans1989.32.737](https://doi.org/10.2320/matertrans1989.32.737).
- [7] Z.-G. Yang, H.-S. Fang, An overview on bainite formation in steels, *Current Opin. Solid State Mater. Sci.* 9 (6) (2005) 277–286, doi: [10.1016/j.cossms.2006.06.005](https://doi.org/10.1016/j.cossms.2006.06.005).
- [8] L.C.D. Fielding, The Bainite Controversy, *Mater. Sci. Technol.* 29 (4) (2013) 383–399, doi: [10.1179/1743284712Y.0000000157](https://doi.org/10.1179/1743284712Y.0000000157).
- [9] F. Caballero, M. Miller, C. Garcia-Mateo, J. Cornide, New experimental evidence of the diffusionless transformation nature of bainite, *J. Alloys Comp.* 577, Supplement 1 (2013) S626–S630, doi: [10.1016/j.jallcom.2012.02.130](https://doi.org/10.1016/j.jallcom.2012.02.130).
- [10] H. Chen, S. van der Zwaag, A general mixed-mode model for the austenite-to-ferrite transformation kinetics in Fe–C–M alloys, *Acta Materialia* 72 (2014) 1–12, doi: [10.1016/j.actamat.2014.03.034](https://doi.org/10.1016/j.actamat.2014.03.034).
- [11] K. Rakha, H. Beladi, I. Timokhina, X. Xiong, S. Kabra, K.-D. Liss, P. Hodgson, On low temperature bainite transformation characteristics using in-situ neutron diffraction and atom probe tomography, *Mater. Sci. Eng. A* 589 (2014) 303–309, doi: [10.1016/j.msea.2013.09.055](https://doi.org/10.1016/j.msea.2013.09.055).
- [12] I.B. Timokhina, K.D. Liss, D. Raabe, K. Rakha, H. Beladi, X.Y. Xiong, P.D. Hodgson, Growth of bainitic ferrite and carbon partitioning during the early stages of bainite transformation in a 2mass studied by *in situ* neutron diffraction, *TEM and APT*, *J. Appl. Crystallogr.* 49 (2) (2016) 399–414, doi: [10.1107/S1600576716000418](https://doi.org/10.1107/S1600576716000418).
- [13] R.F. Hehemann, K.R. Kinsman, H.I. Aaronson, A debate on the bainite reaction, *Metall. Trans.* 3 (5) (1972) 1077–1094, doi: [10.1007/BF02642439](https://doi.org/10.1007/BF02642439).
- [14] I. Timokhina, H. Beladi, X. Xiong, Y. Adachi, P. Hodgson, Nanoscale microstructural characterization of a nanobainitic steel, *Acta Materialia* 59 (14) (2011) 5511–5522, doi: [10.1016/j.actamat.2011.05.024](https://doi.org/10.1016/j.actamat.2011.05.024).
- [15] C. Garcia-Mateo, F.G. Caballero, Ultra-high-strength bainitic steels, *ISIJ Int.* 45 (11) (2005) 1736–1740, doi: [10.2355/isijinternational.45.1736](https://doi.org/10.2355/isijinternational.45.1736).
- [16] S. Singh, H. Bhadeshia, Estimation of bainite plate-thickness in low-alloy steels, *Mater. Sci. Eng. A* 245 (1) (1998) 72–79, doi: [10.1016/S0921-5093\(97\)00701-6](https://doi.org/10.1016/S0921-5093(97)00701-6).
- [17] R. Song, D. Ponge, D. Raabe, J. Speer, D. Matlock, Overview of processing, microstructure and mechanical properties of ultrafine grained BCC steels, *Mater. Sci. Eng. A* 441 (1–2) (2006) 1–17, doi: [10.1016/j.msea.2006.08.095](https://doi.org/10.1016/j.msea.2006.08.095).
- [18] H.K.D.H. Bhadeshia, The first bulk nanostructured metal, *Sci. Technol. Adv. Mater.* 14 (1) (2013) 014202, doi: [10.1088/1468-6996/14/1/014202](https://doi.org/10.1088/1468-6996/14/1/014202).
- [19] K. Nagai, Ultrafine grained steels: basic research and attempts for application, *Can. Metall. Q.* 44 (2) (2005) 187–194, doi: [10.1179/000844305794409463](https://doi.org/10.1179/000844305794409463).
- [20] C. Garcia-Mateo, F.G. Caballero, H.K.D.H. Bhadeshia, Acceleration of low-temperature bainite, *ISIJ Int.* 43 (11) (2003) 1821–1825, doi: [10.2355/isijinternational.43.1821](https://doi.org/10.2355/isijinternational.43.1821).
- [21] T. Sourmail, V. Smanio, Low temperature kinetics of bainite formation in high carbon steels, *Acta Materialia* 61 (7) (2013) 2639–2648, doi: [10.1016/j.actamat.2013.01.044](https://doi.org/10.1016/j.actamat.2013.01.044).
- [22] H. Vettiers, J. Dong, H. Bornas, F. Hoffmann, H.-W. Zoch, Microstructure and fatigue strength of the roller-bearing steel 100Cr6 (SAE 52100) after two-step bainitisation and combined bainitic-martensitic heat treatment, *Int. J. Mater. Res.* 97 (10) (2006) 1432–1440, doi: [10.3139/146.101388](https://doi.org/10.3139/146.101388).
- [23] H. Kawata, M. Takahashi, K. Hayashi, N. Sugiura, N. Yoshinaga, Effect of martensite in initial structure on bainite transformation, *THERMEC, Materials Science Forum*, 638, Trans Tech Publications, 2010, pp. 3307–3312, doi: [10.4028/www.scientific.net/MSF.638-642.3307](https://doi.org/10.4028/www.scientific.net/MSF.638-642.3307).
- [24] W. Gong, Y. Tomota, S. Harjo, Y. Su, K. Aizawa, Effect of prior martensite on bainite transformation in nanobainite steel, *Acta Materialia* 85 (2015) 243–249, doi: [10.1016/j.actamat.2014.11.029](https://doi.org/10.1016/j.actamat.2014.11.029).
- [25] T. Sourmail, V. Smanio, Effect of partial martensite transformation on bainite reaction kinetics in different 1% C steels, *Solid-Solid Phase Transformations in Inorganic Materials, Solid State Phenomena*, 172, Trans Tech Publications, 2011, pp. 821–826, doi: [10.4028/www.scientific.net/SSP.172-174.821](https://doi.org/10.4028/www.scientific.net/SSP.172-174.821).
- [26] A. Navarro-López, J. Sietsma, M.J. Santofimia, Effect of prior athermal martensite on the isothermal transformation kinetics below M_s in a low-C high-Si steel, *Metall. Mater. Trans. A* 47 (3) (2016) 1028–1039, doi: [10.1007/s11661-015-3285-6](https://doi.org/10.1007/s11661-015-3285-6).
- [27] S. Samanta, P. Biswas, S. Giri, S.B. Singh, S. Kundu, Formation of bainite below the m_s temperature: Kinetics and crystallography, *Acta Materialia* 105 (2016) 390–403, doi: [10.1016/j.actamat.2015.12.027](https://doi.org/10.1016/j.actamat.2015.12.027).
- [28] S. Samanta, P. Biswas, S.B. Singh, Analysis of the kinetics of bainite formation below the m_s temperature, *Scripta Materialia* 136 (2017) 132–135, doi: [10.1016/j.scriptamat.2017.04.030](https://doi.org/10.1016/j.scriptamat.2017.04.030).
- [29] A. Navarro-López, J. Hidalgo, J. Sietsma, M. Santofimia, Characterization of bainitic/martensitic structures formed in isothermal treatments below the m_s temperature, *Mater. Characteriz.* 128 (2017) 248–256, doi: [10.1016/j.matchar.2017.04.007](https://doi.org/10.1016/j.matchar.2017.04.007).
- [30] J.G. Speer, B.C. De Cooman, D.H. Kim, The isothermal transformation of low-alloy low-C CMNSI steels below m_s , *PRICM7, Materials Science Forum*, 654, Trans Tech Publications, 2010, pp. 98–101, doi: [10.4028/www.scientific.net/MSF.654-656.98](https://doi.org/10.4028/www.scientific.net/MSF.654-656.98).
- [31] M. Oka, H. Okamoto, Swing back in kinetics near m_s in hypereutectoid steels, *Metall. Trans. A* 19 (3) (1988) 447–452, doi: [10.1007/BF02649258](https://doi.org/10.1007/BF02649258).
- [32] D. Quidort, Y.J.M. Brechet, A model of isothermal and non isothermal transformation kinetics of bainite in 0.5% C steels, *ISIJ Int.* 42 (9) (2002) 1010–1017, doi: [10.2355/isijinternational.42.1010](https://doi.org/10.2355/isijinternational.42.1010).
- [33] G.I. Rees, H.K.D.H. Bhadeshia, Bainite transformation kinetics Part 1 Modified model, *Mater. Sci. Technol.* 8 (11) (1992) 985–993, doi: [10.1179/mst.1992.8.11.985](https://doi.org/10.1179/mst.1992.8.11.985).
- [34] M.J. Santofimia, F.G. Caballero, C. Capdevila, C. Garcia-Mateo, C.G. de Andres, Evaluation of displacive models for bainite transformation kinetics in steels, *Mater. Trans.* 47 (6) (2006) 1492–1500, doi: [10.2320/matertrans.47.1492](https://doi.org/10.2320/matertrans.47.1492).
- [35] H.K.D.H. Bhadeshia, *Bainite: Overall Transformation Kinetics*, *J. Physique* 43 (1982) 443–448.
- [36] N.A. Chester, H.K.D.H. Bhadeshia, Mathematical modelling of bainite transformation kinetics, *J. Phys. IV France* 07 (C5) (1997) 41–46, doi: [10.1051/jp4:1997506](https://doi.org/10.1051/jp4:1997506).
- [37] S.M.C. van Bohemen, J. Sietsma, Modeling of isothermal bainite formation based on the nucleation kinetics, *Int. J. Mater. Res.* 99 (7) (2008) 739–747, doi: [10.3139/146.101695](https://doi.org/10.3139/146.101695).
- [38] A.M. Ravi, J. Sietsma, M.J. Santofimia, Exploring bainite formation kinetics distinguishing grain-boundary and autocatalytic nucleation in high and low-si steels, *Acta Materialia* 105 (2016) 155–164, doi: [10.1016/j.actamat.2015.11.044](https://doi.org/10.1016/j.actamat.2015.11.044).
- [39] S.M.C. van Bohemen, Modeling start curves of bainite formation, *Metall. Mater. Trans. A* 41 (2) (2010) 285–296, doi: [10.1007/s11661-009-0106-9](https://doi.org/10.1007/s11661-009-0106-9).
- [40] D. Quidort, Y. Brechet, The role of carbon on the kinetics of bainite transformation in steels, *Scripta Materialia* 47 (3) (2002) 151–156, doi: [10.1016/S1359-6462\(02\)00121-5](https://doi.org/10.1016/S1359-6462(02)00121-5).
- [41] H.K.D.H. Bhadeshia, A rationalisation of shear transformations in steels, *Acta Metallurgica* 29 (6) (1981) 1117–1130, doi: [10.1016/0001-6160\(81\)90063-8](https://doi.org/10.1016/0001-6160(81)90063-8).
- [42] A.M. Ravi, J. Sietsma, M.J. Santofimia, Bainite formation kinetics in steels and the dynamic nature of the autocatalytic nucleation process, *Scripta Materialia* 140 (2017) 82–86, doi: [10.1016/j.scriptamat.2017.06.051](https://doi.org/10.1016/j.scriptamat.2017.06.051).
- [43] B. Bramfitt, A. Benscoter, *Metallographer's Guide: Practice and Procedures for Irons and Steels*, ASM International, 2001.
- [44] S.M.C. van Bohemen, J. Sietsma, Effect of composition on kinetics of athermal martensite formation in plain carbon steels, *Mater. Sci. Technol.* 25 (8) (2009) 1009–1012, doi: [10.1179/174328408X365838](https://doi.org/10.1179/174328408X365838).

- [45] N. Takayama, G. Miyamoto, T. Furuhashi, Effects of transformation temperature on variant pairing of bainitic ferrite in low carbon steel, *Acta Materialia* 60 (5) (2012) 2387–2396, doi: [10.1016/j.actamat.2011.12.018](https://doi.org/10.1016/j.actamat.2011.12.018).
- [46] G. Miyamoto, N. Takayama, T. Furuhashi, Accurate measurement of the orientation relationship of lath martensite and bainite by electron backscatter diffraction analysis, *Scripta Materialia* 60 (12) (2009) 1113–1116, doi: [10.1016/j.scriptamat.2009.02.053](https://doi.org/10.1016/j.scriptamat.2009.02.053).
- [47] H. Bhadeshia, A. Waugh, Bainite: an atom-probe study of the incomplete reaction phenomenon, *Acta Metallurgica* 30 (4) (1982) 775–784, doi: [10.1016/0001-6160\(82\)90075-X](https://doi.org/10.1016/0001-6160(82)90075-X).
- [48] F. Caballero, M. Miller, S. Babu, C. Garcia-Mateo, Atomic scale observations of bainite transformation in a high carbon high silicon steel, *Acta Materialia* 55 (1) (2007) 381–390, doi: [10.1016/j.actamat.2006.08.033](https://doi.org/10.1016/j.actamat.2006.08.033).